Electronic Supporting Information (ESI):

Thermally and photoresponsive luminescent single-molecule magnet based on dysprosium-anthracene: effect of temperature on anthracene photocycloaddition

Xiu-Fang Ma,[a‡] Xinlan Hou,[b‡] Ye-Hui Qin,[a] Qian Teng,[a] Song-Song Bao,[a] Yuxi Tian*[b] and Li-Min Zheng*[a]

[a.] State Key Laboratory of Coordination Chemistry, School of Chemistry and Chemical Engineering, Collaborative Innovation Center of Advanced Microstructures, Nanjing University, Nanjing University, Nanjing 210023, P. R. China.

[b.] Key Laboratory of Mesoscopic Chemistry of MOE, School of Chemistry and Chemical Engineering, School of Chemistry and Chemical Engineering, Nanjing University, Nanjing 210023, China.

E-mail: lmzheng@nju.edu.cn
tyx@nju.edu.cn

Content

I. Experimental section

Materials and physical measurements. The 9-diethyl-phosphonomethylanthracene (depma) were synthesized according to the literature.[1] All other starting reagents and solvents were obtained from commercial sources and used as received without further purification. The C, H and N microanalyses were carried out on PE 240C analyzer. The infrared (IR) spectra were measured in the range 4000-400 cm^{-1} using KBr pellets on Bruker Tensor 27 spectrometer. The thermogravimetric (TG) analyses were conducted on a Mettler Toledo TGA/DSC 1 instrument in the range of 30-600 °C under N_2 atmosphere at a heating rate of 5 °C min^{-1}. Powder X-ray diffraction (PXRD) data were recorded on a Bruker D8 advance diffractometer with Cu-K_α radiation in a range of 5-50° at room temperature. The differential scanning calorimetry (DSC) measurement was conducted on a Mettlr DSC823e instrument. The UV/Vis spectra were measured on a Perkin Elmer Lambda 950 UV/VIS/NIR spectrometer using powder samples. The photochemical reactions were performed upon irradiation with LED UV light in 395 nm. Variable temperature fluorescence spectra were measured on a Horiba-JY HR Evolution using single crystal samples in the range 77-300 K. Time resolved fluorescence and quantum yield measurements were performed on an Edinburgh FLS 980 at room temperature. Fluorescence spectra at room temperature with UV illumination were determined on an Edinburgh FLS 980. Fluorescence spectra in the range 77-300 K with UV illumination were measured on a Horiba-JY HR Evolution using single crystal samples. The dc and ac magnetic susceptibility data were collected on polycrystalline samples by Quantum Design vibrating sample magnetometer (VSM). The ^1H NMR spectra were recorded on BRUKER AVANCE III 400 MHz spectrometer at different temperature with **1DySeCN** and **2DySeCN** dissolved in DMSO-d_6.

Synthesis of $Dy(SeCN)_2(NO_3)(depma)_2(4\text{-}hpy)_2$ (1DySeCN). $Dy(NO_3)_3{\cdot}6H_2O$ (0.05 mmol, 22.8 mg) and KSeCN (0.11 mmol, 15.8 mg) were dissolved in 10 mL of CH_3CN solvent, stirred for 30 min and then filtered to remove the red precipitate，the 4-hpy (1.1 mmol, 10. 4 mg) and depma (1.0 mmol, 32.9 mg) were added and stirred about 30 min. Then, after filtered, the clear solution was subject to slow evaporation for three days to give block yellow crystals. Yield: 32.6 mg, yield: 50.81%. Elemental anal. Calcd for $C_{50}H_{52}DyN_5O_{11}P_2Se_2$ (F_W = 1281.4 g mol^{-1}, %): C, 46.87; H, 4.09; N, 5.47. Found (%): C, 46.79, H, 4.05, N, 5.52.

Synthesis of $Dy(SeCN)_2(NO_3)(depma_2)(4\text{-}hpy)_2$ (2DySeCN). The polycrystalline samples of **1DySeCN** are exposed to 395 nm UV light (powder of 100 mW cm^{-2}) for 12 hours to give corresponding product of **2DySeCN** for characterization and magnetic measurement. Elemental anal. Calcd for $C_{50}H_{52}DyN_5O_{11}P_2Se_2$ (F_W = 1281.4 g mol^{-1}, %): C, 46.87, H, 4.09, N, 5.47; Found (%): C, 46.72, H, 4.02, N, 5.42.

Synthesis of $Dy_{0.05}Y_{0.95}(SeCN)_2(NO_3)(depma)_2(4\text{-}hpy)_2$ (1DySeCN@Y). The diluted samples **1DySeCN@Y** was synthesized with the same ways described as **1DySeCN** except that $Dy(NO_3)_3{\cdot}6H_2O$ was replaced by a mixture of $Dy(NO_3)_3{\cdot}6H_2O$ (0.0025 mmol, 1.15 mg) and $Y(NO_3)_3{\cdot}6H_2O$(0.0475 mmol, 18.3 mg) in a molar ratios of 1:19. Yield: 34.5mg, yield: 53.50%. Elemental anal. Calcd for $C_{50}H_{52}Dy_{0.05}Y_{0.95}N_5O_{11}P_2Se_2$ (F_W = 1121.4 g mol^{-1}, %): C, 49.57, H, 4.33, N, 5.78; Found (%): C, 49.52, H, 4.39, N, 5.71. The dilution ratios were checked by the ICP-AES analyses (Dy: Y= 1:18.3) and the phase purity of was **1DySeCN@Y** confirmed by the powder XRD.

Synthesis of $Dy_{0.05}Y_{0.95}(SeCN)_2(NO_3)(depma_2)(4\text{-}hpy)_2$ (2DySeCN@Y). The polycrystalline samples of **1DySeCN@Y** are exposed to 395 nm UV light for 12 hours to give corresponding product of **2DySeCN@Y** for characterization and magnetic measurement. Elemental anal. Calcd for 128 $C_{50}H_{52}Dy_{0.05}Y_{0.95}N_5O_{11}P_2Se_2$ (F_W = 1121.4 g mol^{-1}, %): C, 49.57, H, 4.33, N, 5.78; Found (%): C, 49.48, H, 4.42, N, 5.72.

X-ray Crystallography. Single crystals were used for data collections on Bruker D8 Venture or APEX duo diffractometers using graphite-monochromated Mo-Kα radiation (λ = 0.71073 Å). The data were integrated using the Siemens SAINT program,[2] with the intensities corrected for Lorentz factor, polarization, air absorption, and absorption due to variation in the path length through the detector faceplate. Empirical absorption corrections were applied using the SADABS program.[3] The structures were solved and refined on F^2 by full-matrix least squares using Olex 2.1.[4] All the non-hydrogen atoms were refined anisotropically. All hydrogen atoms were located in a difference map, added geometrically, and isotropically refined with a riding model. The residual electron densities were of no chemical significance. CCDC 2424230 (**1DySeCN-130**), 2421525 (**1DySeCN-193**), 2421526 (**1DySeCN-293**), 2421527 (**2DySeCN-193**), 2424231 (**2DySeCN-293**) contain the supplementary crystallographic data for this paper. These data can be obtained free of charge from the Cambridge Crystallographic Data Centre via www.ccdc.cam.ac.uk/data_request/cif. Detailed crystal data and structural refinement parameters are listed in Table S1. It is worth mentioning that despite multiple attempts at collecting single-crystal data for **1DySeCN-130**, the obtained data exhibited relatively low completeness. This may be attributed to the impact of the low-temperature environment on the stability of the crystal or the quality of diffraction, resulting in higher background noise or weaker diffraction signals during data collection.

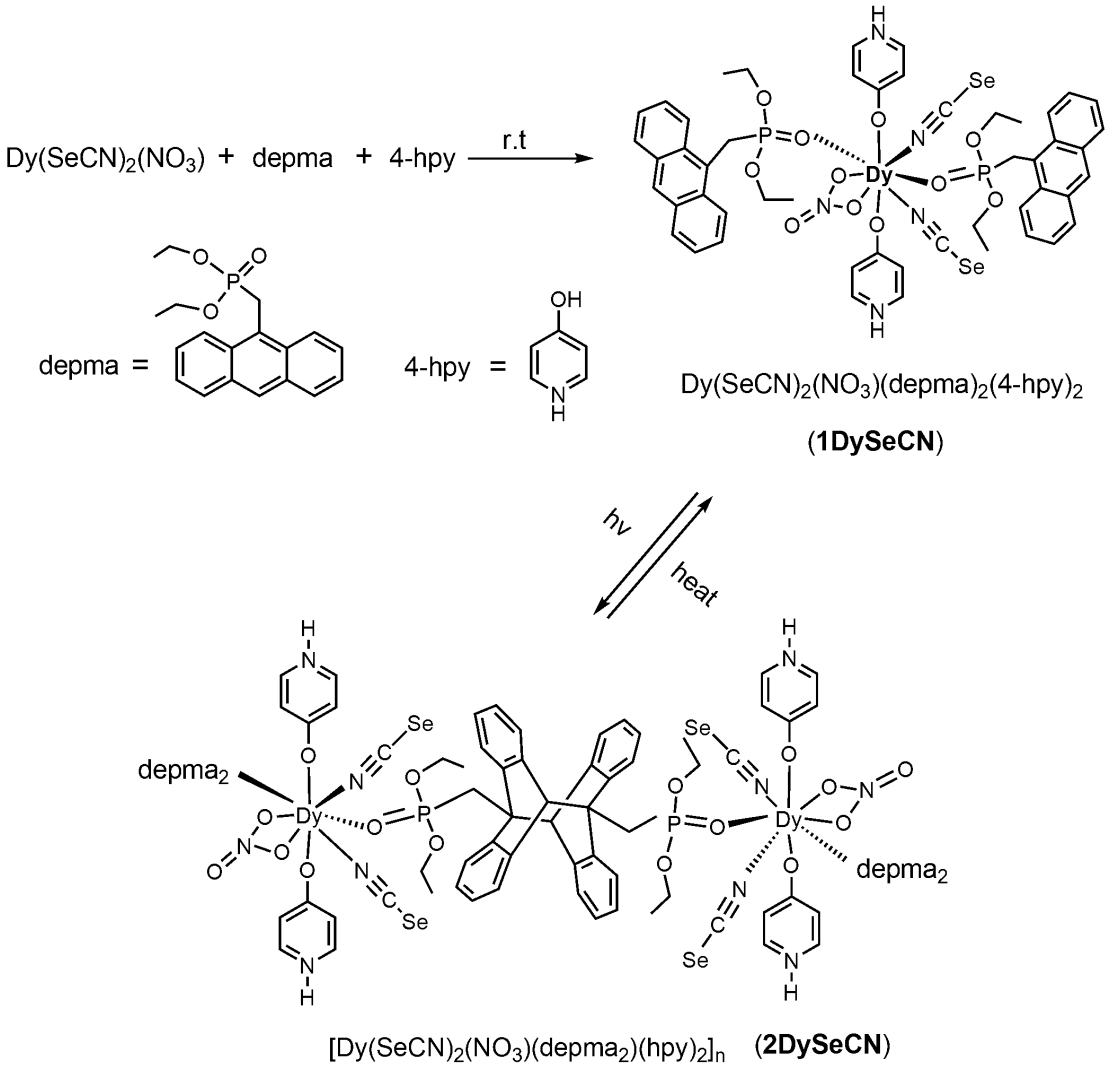

Scheme S1. Preparation of compounds **1DySeCN** and **2DySeCN**.

II. Crystal structures of 1DySeCN and 2DySeCN

Table S1. Crystallographic data for compounds **1DySeCN** and **2DySeCN** under different temperature.

	1DySeCN-130	**1DySeCN -193**	**1DySeCN -293**	**2DySeCN-193**	**2DySeCN-293**
T (K)	130	193	293	193	293
Empirical formula			$C_{50}H_{52}DyN_5O_{11}P_2Se_2$		
Crystal system	triclinic	triclinic	monoclinic	monoclinic	monoclinic
Space group	*P*-1	*P*-1	$P2_1/m$	$P2_1/m$	$P2_1/m$
a (Å)	9.7055(12)	9.6729(5)	9.7539(12)	9.5847(12)	9.585(9)
b (Å)	11.1138(13)	11.1667(6)	25.787(3)	25.809(3)	25.97(2)
c (Å)	25.416(3)	25.6156(16)	11.2182(14)	11.2751(13)	11.340(12)
α (º)	90.469(3)	90.315(2)	90	90	90
β (º)	92.518(4)	92.411(2)	111.587(4)	112.946(3)	112.620(19)
γ (º)	112.134(3)	112.001(2)	90	90	90
V (Å^3)	2536.1(5)	2562.4(3)	2623.8(5)	2568.4(6)	2606(4)
Z	2	2	2	2	2
ρ_{calcd} (g cm^{-3})	1.678	1.663	1.586	1.657	1.633
μ (mm^{-1})	3.036	3.005	2.934	2.998	2.955
F(000)	1278	1283.2	1199.2	1278.0	1278.0
R_{int}	0.0314	0.0426	0.0810	0.0894	0.1445
R_1, wR_2 [I >2σ(I)][a]	0.0582, 0.1559	0.0363, 0.0943	0.0605, 0.1348	0.0858, 0.1817	0.0859, 0.1556
R_1, wR_2 (all data)[a]	0.0610, 0.1582	0.0409, 0.0974	0.1095, 0.1653	0.1493, 0.2206	0.1658, 0.1919
goodness-of-fit	1.142	1.040	1.060	1.039	1.115
CCDC	2424230	2421525	2421526	2421527	2424231

[a] $R1 = \Sigma||F_o| - |F_c||/\Sigma|F_o|$, $wR_2 = [\Sigma w(F_o^2 - F_c^2)^2/\Sigma w(F_o^2)^2]^{1/2}$

Table S2. Selected bond lengths (Å) and angle (°) for **1DySeCN** and **2DySeCN** at different temperature.

1DySeCN-130			
Dy1-O1	2.333(6)	O4-Dy1-O10	71.4(2)
Dy1-O4	2.310(6)	O4-Dy1-N2	145.6(2)
Dy1-O7	2.227(6)	O4-Dy1-N1	74.0(2)
Dy1-O8	2.243(6)	O7-Dy1-O8	162.2(2)
Dy1-O9	2.507(5)	O7-Dy1-O9	73.3(2)
Dy1-O10	2.557(5)	O7-Dy1-O10	124.1(2)
Dy1-N1	2.462(7)	O7-Dy1-N1	82.9(3)
Dy1-N2	2.474(7)	O7-Dy1-N2	83.1(3)
O1-Dy1-O4	139.4(2)	O8-Dy1-O9	124.4(2)
O1-Dy1-O7	89.2(2)	O8-Dy1-O10	73.6(2)
O1-Dy1-O8	95.5(2)	O8-Dy1-N1	81.8(3)
O1-Dy1-O9	72.7(2)	O8-Dy1-N2	83.5(3)
O1-Dy1-O10	73.8(2)	O9-Dy1-O10	50.81(17)
O1-Dy1-N1	74.9(3)	O9-Dy1-N1	139.7(2)
O1-Dy1-N2	146.3(2)	O9-Dy1-N2	134.6(2)
O4 -Dy1-O7	93.2(2)	O10-Dy1-N1	137.7(2)
O4-Dy1-O8	94.3(2)	O10-Dy1-N2	136.4(2)
O4-Dy1-O9	69.3(2)	N1-Dy1-N2	71.6(3)
1DySeCN-193			
Dy1-O1	2.328(3)	O4-Dy1-O10	71.29(9)
Dy1-O4	2.317(3)	O4-Dy1-N2	145.75(12)
Dy1-O7	2.228(2)	O4-Dy1-N1	73.79(11)
Dy1-O8	2.240(2)	O7-Dy1-O8	161.96(11)
Dy1-O9	2.515(3)	O7-Dy1-O9	74.36(9)
Dy1-O10	2.563(2)	O7-Dy1-O10	124.59(9)
Dy1-N1	2.468(3)	O7-Dy1-N1	83.11(12)
Dy1-N2	2.464(4)	O7-Dy1-N2	83.13(12)
O1-Dy1-O4	139.48(10)	O8-Dy1-O9	123.66(9)
O1-Dy1-O7	89.51(10)	O8-Dy1-O10	73.43(9)
O1-Dy1-O8	95.52(10)	O8-Dy1-N1	82.02(11)
O1-Dy1-O9	71.90(9)	O8-Dy1-N2	83.13(12)
O1-Dy1-O10	74.29(8)	O9-Dy1-O10	50.23(7)
O1-Dy1-N1	74.62(11)	O9-Dy1-N1	139.13(11)
O1-Dy1-N2	146.42(11)	O9-Dy1-N2	135.74(10)
O4 -Dy1-O7	92.75(11)	O10-Dy1-N1	137.85(11)
O4-Dy1-O8	94.58(11)	O10-Dy1-N2	135.68(11)
O4-Dy1-O9	69.87(10)	N1-Dy1-N2	71.96(13)
1DySeCN-293			
Dy1-O1	2.313(6)	O1A -Dy1-O10	73.07(16)

Dy1-O1A	2.313(6)	O1A -Dy1-N1A	145.6(3)
Dy1-O7	2.208(9)	O1A -Dy1-N1	73.7(3)
Dy1-O8	2.231(8)	O7-Dy1-O8	163.2(4)
Dy1-O9	2.528(9)	O7-Dy1-O9	74.4(3)
Dy1-O10	2.576(8)	O7-Dy1-O10	123.7(3)
Dy1-N1	2.462(9)	O7-Dy1-N1	83.3(3)
Dy1-N1A	2.462(9)	O7-Dy1-N1A	83.3(3)
O1-Dy1-O1A	140.5(3)	O8-Dy1-O9	122.4(3)
O1-Dy1-O7	91.1(2)	O8-Dy1-O10	73.1(3)
O1-Dy1-O8	94.6(2)	O8-Dy1-N1	83.1(3)
O1-Dy1-O9	71.33(17)	O8-Dy1-N1A	83.1(3)
O1-Dy1-O10	73.07(16)	O9-Dy1-O10	49.3(2)
O1-Dy1-N1	73.7(3)	O9-Dy1-N1	137.7(2)
O1-Dy1-N1A	145.6(3)	O9-Dy1-N1A	137.7(2)
O1A -Dy1-O7	91.1(2)	O10-Dy1-N1	137.0(2)
O1A -Dy1-O8	94.6(2)	O10-Dy1-N1A	137.0(2)
O1A -Dy1-O9	71.33(17)	N1-Dy1-N1A	71.9(4)
2DySeCN-193			
Dy1-O1	2.314(10)	O1A -Dy1-O10	74.3(3)
Dy1-O1A	2.314(10)	O1A -Dy1-N1A	144.5(5)
Dy1-O7	2.211(12)	O1A -Dy1-N1	75.0(5)
Dy1-O8	2.236(10)	O7-Dy1-O8	162.4(6)
Dy1-O9	2.546(10)	O7-Dy1-O9	75.1(5)
Dy1-O10	2.532(10)	O7-Dy1-O10	124.5(5)
Dy1-N1	2.452(11)	O7-Dy1-N1	86.0(6)
Dy1-N1A	2.452(12)	O7-Dy1-N1A	86.0(6)
O1-Dy1-O1A	140.2(5)	O8-Dy1-O9	122.4(5)
O1-Dy1-O7	89.0(4)	O8-Dy1-O10	73.1(5)
O1-Dy1-O8	96.8(4)	O8-Dy1-N1	79.6(6)
O1-Dy1-O9	70.5(3)	O8-Dy1-N1A	79.6(6)
O1-Dy1-O10	74.3(3)	O9-Dy1-O10	49.4(4)
O1-Dy1-N1	75.0(5)	O9-Dy1-N1	140.6(4)
O1-Dy1-N1A	144.5(5)	O9-Dy1-N1A	140.6(4)
O1A -Dy1-O7	89.0(4)	O10-Dy1-N1	135.5(5)
O1A -Dy1-O8	96.8(4)	O10-Dy1-N1A	135.5(5)
O1A -Dy1-O9	70.5(3)	N1-Dy1-N1A	69.6(8)
2DySeCN-293			
Dy1-O1	2.307(7)	O1A -Dy1-O10	74.3(3)
Dy1-O1A	2.307(7)	O1A -Dy1-N1A	144.5(5)
Dy1-O7	2.222(11)	O1A -Dy1-N1	75.0(5)
Dy1-O8	2.250(10)	O7-Dy1-O8	162.4(6)
Dy1-O9	2.529(10)	O7-Dy1-O9	75.1(5)
Dy1-O10	2.568(10)	O7-Dy1-O10	124.5(5)

Dy1-N1	2.456(11)	O7-Dy1-N1	85.5(4)
Dy1-N1A	2.456(11)	O7-Dy1-N1A	85.5(4)
O1-Dy1-O1A	141.1(4)	O8-Dy1-O9	120.6(4)
O1-Dy1-O7	88.9(2)	O8-Dy1-O10	71.3(4)
O1-Dy1-O8	96.6(2)	O8-Dy1-N1	80.6(4)
O1-Dy1-O9	70.89(19)	O8-Dy1-N1A	80.6(4)
O1-Dy1-O10	74.96 (19)	O9-Dy1-O10	49.2(3)
O1-Dy1-N1	74.8(3)	O9-Dy1-N1	141.1(3)
O1-Dy1-N1A	143.6(3)	O9-Dy1-N1A	141.1(3)
O1A -Dy1-O7	88.9(2)	O10-Dy1-N1	135.5(3)
O1A -Dy1-O8	96.6(2)	O10-Dy1-N1A	135.5(3)
O1A -Dy1-O9	70.89(19)	N1-Dy1-N1A	69.0 (5)

1DySeCN-293: 1+X,1/2-Y,+Z; **1DySeCN-193**: 1+X,1/2-Y,+Z; **2DySeCN-293**: 1+X,3/2-Y,+Z; **2DySeCN-193**: 1+X,3/2-Y,+Z;

Table S3. Continuous Shape Measure (CShM) analyses of dysprosium geometries for **1DySeCN** and **2DySeCN** at different temperature using the SHAPE2.1 Software.

Geometry	Symmetry	**1DySeCN-193**	**1DySeCN-293**	**2DySeCN-193**	**2DySeCN-293**
Hexagonal bipyramid	D_{6h}	13.720	13.942	13.720	13.560
Cube	O_h	13.712	13.559	13.712	13.528
Square antiprism	D_{4d}	4.688	4.156	4.688	4.808
Triangular dodecahedron	D_{2d}	2.219	1.803	2.219	2.266
Johnson gyrobifastigium J26	D_{2d}	10.598	10.609	10.598	10.383
Johnson elongated triangular bipyramid J14	D_{3h}	25.936	26.950	25.936	25.972
Biaugmented trigonal prism	C_{2v}	3.147	3.229	3.147	3.253
Biaugmented trigonal prism	C_{2v}	2.999	3.049	2.999	3.042
Snub diphenoid J84	D_{2d}	2.003	1.810	2.003	2.026
Triakis tetrahedron	T_d	14.510	14.343	14.510	14.323
Elongated trigonal bipyramid	D_{3h}	23.431	24.379	23.431	23.343

Table S4. The parameters of H-bonding for **1DySeCN** and **2DySeCN** at different temperature.

Compounds	D-H···A	dH···A (Å)	dD···A (Å)	AngleD-
1DySeCN-293	N3-H3···Se1	3.02	3.66	130.8
	N4-H4···O11	1.99	2.90	161.9
	C2A-H22···O10	2.69	3.47	140.8
	C26-H26···O11	2.71	3.22	113.4
1DySeCN-193	N3-H3···Se1	3.10	3.63	120.7
	N3-H3···Se2	2.81	3.50	136.3
	N4-H4···O11	1.96	2.83	168.9
	C22-H22···O10	2.67	3.18	114.1
	C26-H26···O11	2.69	3.44	135.7
2DySeCN-293	N3-H3···Se1	2.63	3.36	138.7
	N4-H4···O11	2.17	2.99	157.9
	C22-H22···O10	2.76	3.58	147.4
	C26-H26···O11	2.57	3.15	118.8
2DySeCN-193	N3-H3···Se1	3.10	3.64	121.6
	N4-H4···O11	2.05	2.89	157.9
	C22-H22···O10	2.80	3.61	143.3
	C26-H26···O11	2.50	3.08	119.8

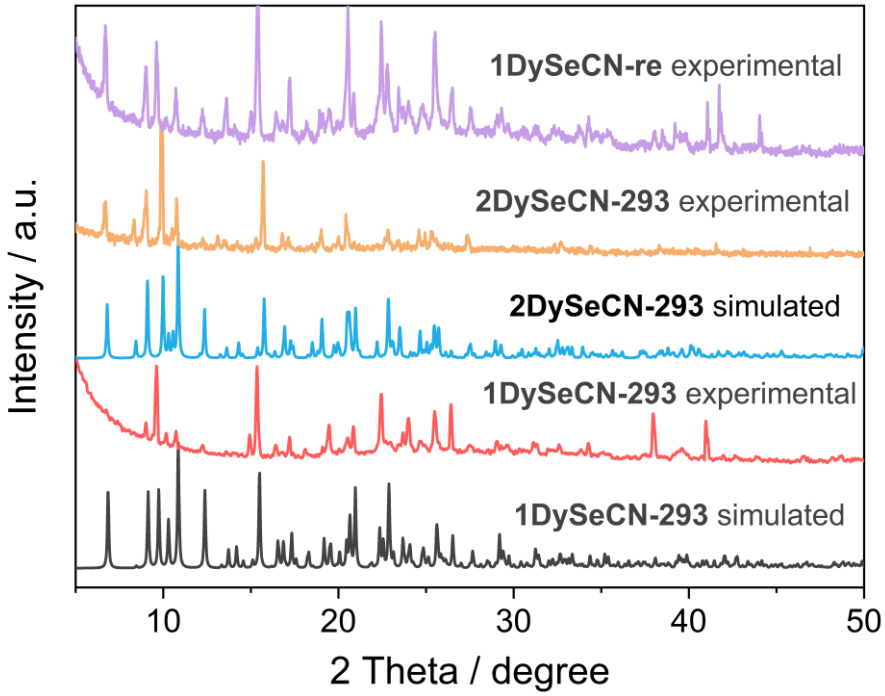

Figure S1. The PXRD patterns for powder samples of **1DySeCN**, **2DySeCN** and **1DySeCN-re** compared with their simulated patterns from corresponding crystal structure. The irradiation of **1DySeCN** upon 395 nm UV light for 12 hours gave the sample **2DySeCN**. **1DySeCN-re** was formed by heating **2DySeCN** at 105°C for 30 min.

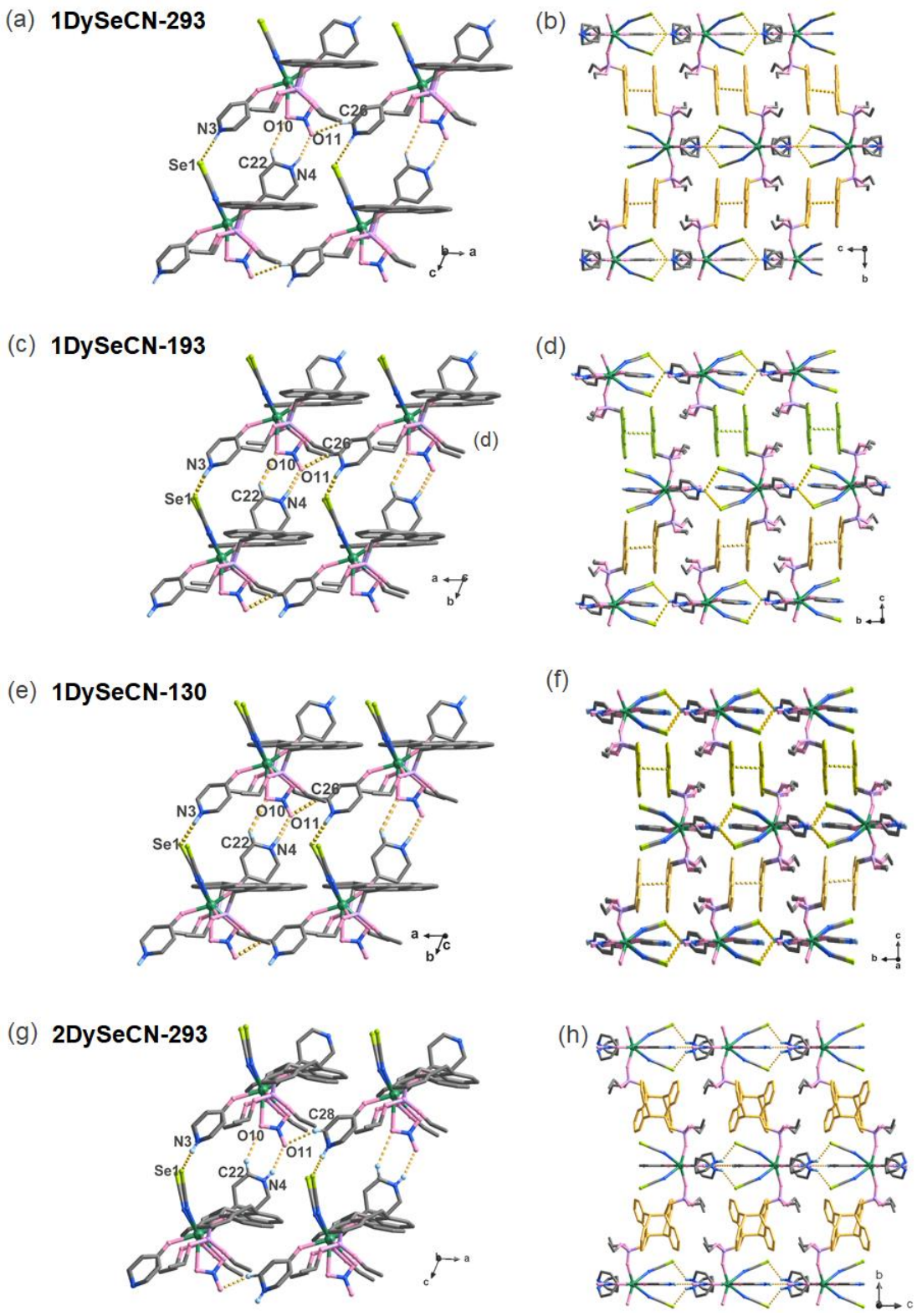

Figure S2. The stacking structure for compounds **1DySeCN-293** (a, b), **1DySeCN-193** (c, d) **1DySeCN-130** (e, f) and **2DySeCN-293** (g, h).

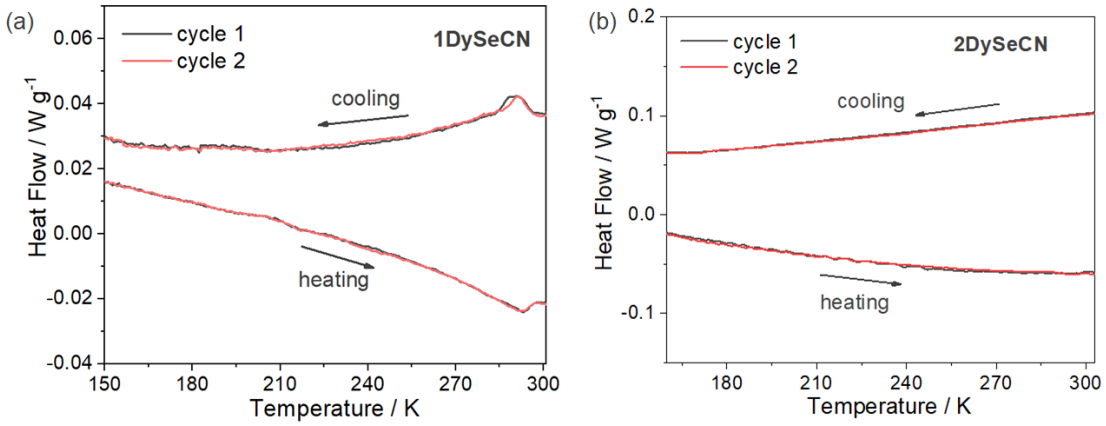

Figure S3. The DSC curves of **1DySeCN** (a) and **2DySeCN** (b) in range of 150-303 K at a scan speed of 5 °C/min for cooling-heating cycles.

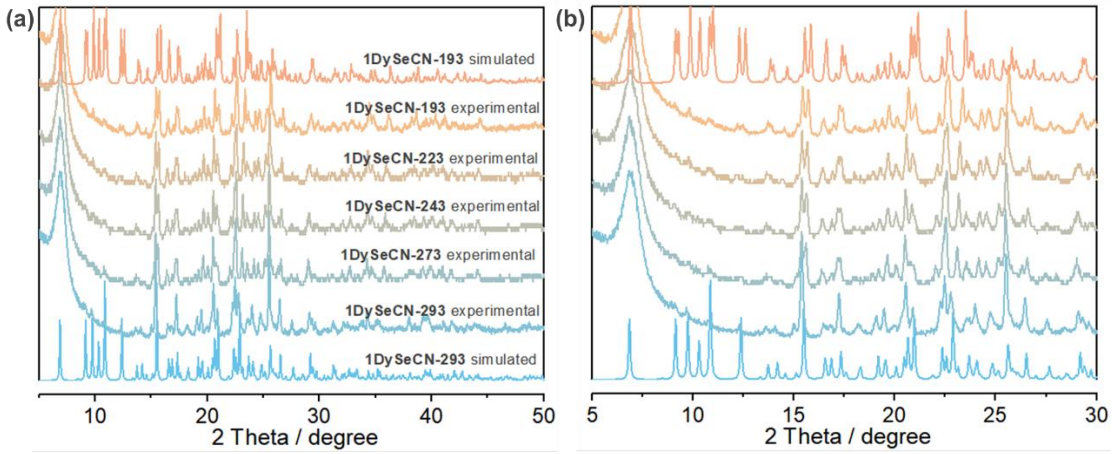

Figure S4. Variable-temperature PXRD patterns of **1DySeCN** powder samples, with a scanning range of 5–50° (left) and 5–30° (right).

It is noteworthy that these patterns were recorded in another instrument of the same type (Bruker D8 advance diffractometer) equipped with a variable temperature facility. The broadening of the peak at 6.9 ° is observed even at 293 K, attributed to the instrument error. The new peak appearing at 15.7 ° below 273 K, confirms the occurrence of phase transition. The overall PXRD pattern of **1DySeCN-193** agrees with that simulated from the single-crystal data of **1DySeCN-193**.

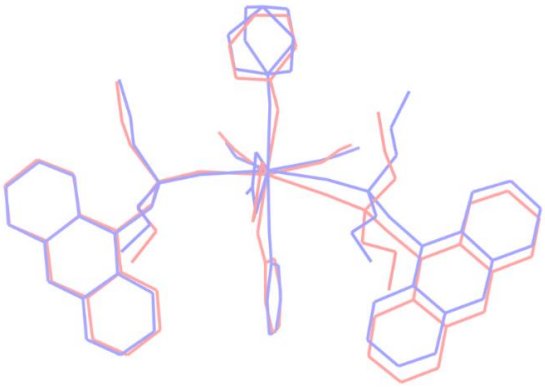

Figure S5. Overlay of the molecular structures of complexes **1DySeCN-293** (purple) and **1DySeCN-193** (red).

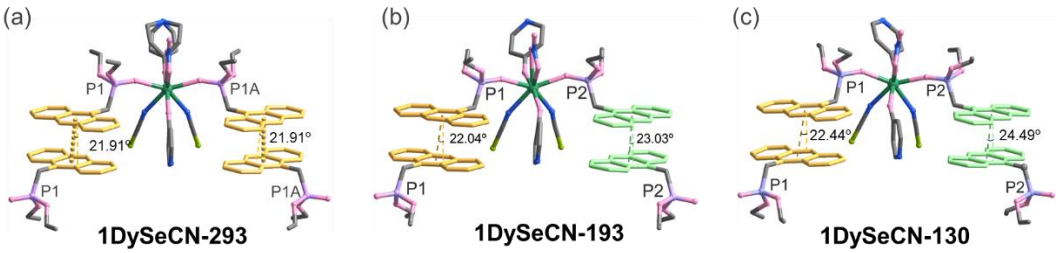

Figure S6. The slipping angles between the anthracene units of **1DySeCN-293**, **1DySeCN-193** and **1DySeCN-130**.

III. Photophysical properties and photoinduced SC-SC structural transformation of 1DySeCN at room temperature

Table S5. The transient luminescent lifetime (τ) at room temperature for **1DySeCN** and **2DySeCN** excited at 365 nm for short nanosecond lifetime and 370 nm for long microsecond lifetime, given by fitting their photoluminescent decay curves to single or double exponential decay equation via the software DAS6 attached to Fluorolog-3 spectrofluorometer (Horiba Scientific).

Compound	λ_{em} / nm	τ_1 / ns (f_1)	τ_2 / ns (f_2)	$\tau_{average}$ / ns	χ^2
1DySeCN	550 (300 K)	13.86 (12.7%)	27.02 (87.3%)	25.35	1.07
	515 (77 K)	32.17		32.17	1.12
2DySeCN	424	0.85 (57.43%)	4.34 (42.57%)	2.34	1.21
	446	1.11 (44.98%)	6.68 (55.02%)	4.17	1.16
	555	1.78 (7.31%)	12.9 (92.69%)	12.09	0.98
	575	1.16 (55.81%)	14.39 (44.19%)	7.01 μs	1.18

Table S6. The cell parameters of reversal single-crystal-to-single-crystal (SC-SC) transformation between compounds **1DySeCN-293** and **2DySeCN-293** up to 5 times.

Cycle	compound	Crystal system	Space group	a / Å	b / Å	c / Å	β / °	V / Å^3
1	**1DySeCN -293**	monoclinic	$P2_1/m$	9.74	25.78	11.26	111.79	2621
	2DySeCN -293	monoclinic	$P2_1/m$	9.62	25.92	11.40	112.65	2638
2	**1DySeCN -293**	monoclinic	$P2_1/m$	9.77	25.70	11.22	111.78	2617
	2DySeCN -293	monoclinic	$P2_1/m$	9.63	26.10	11.34	112.94	2640
3	**1DySeCN -293**	monoclinic	$P2_1/m$	9.72	25.76	11.24	111.87	2623
	2DySeCN -293	monoclinic	$P2_1/m$	9.65	25.95	11.37	112.07	2641
4	**1DySeCN -293**	monoclinic	$P2_1/m$	9.71	25.81	11.33	112.11	2619
	2DySeCN -293	monoclinic	$P2_1/m$	9.64	26.07	11.42	112.67	2647
5	**1DySeCN -293**	monoclinic	$P2_1/m$	9.72	25.74	11.34	112.09	2625
	2DySeCN -293	monoclinic	$P2_1/m$	9.68	25.94	11.77	112.69	2640

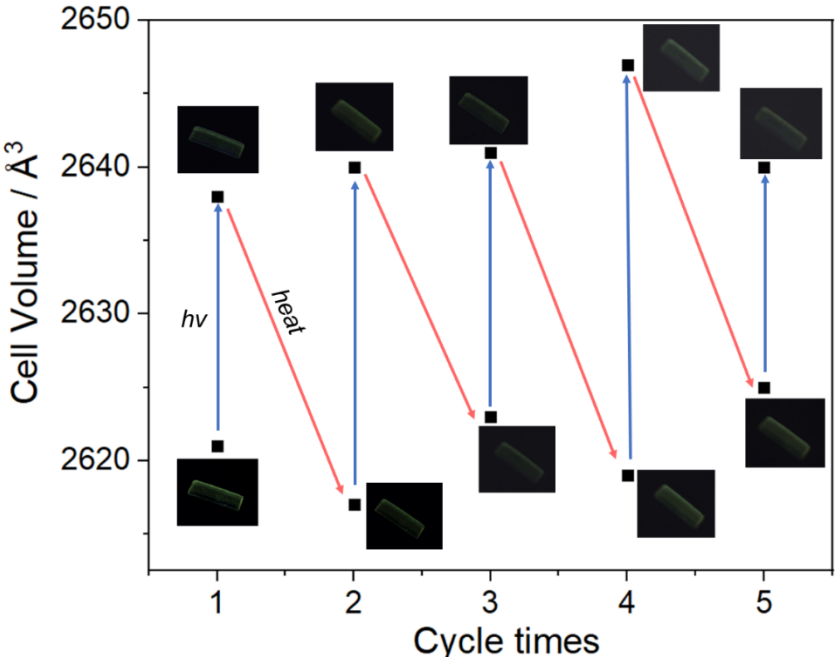

Figure S7. Plot of cell volume vs. time for a single crystal of **1DySeCN** upon UV light irradiation at 395 nm (blue arrow) and then heating at 105 °C (red arrow). Inset: Photographs of a single crystal of **1DySeCN** upon UV light irradiation at 395 nm and then heating at 105°C. The process was repeated for 5 times, accompanied with reversal SC-SC structural transformations between **1DySeCN** and **2DySeCN**.

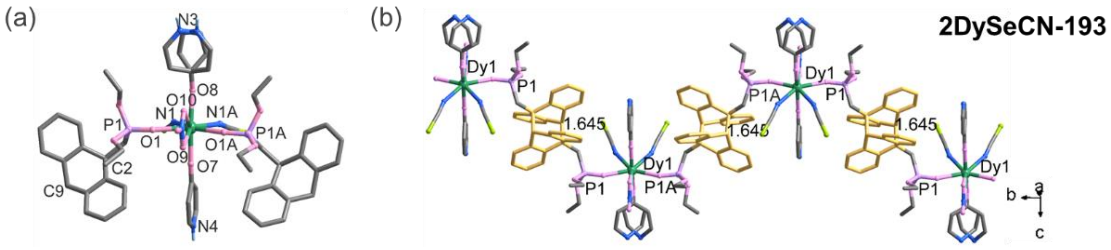

Figure S8. The molecule structures (a) and 1D chain (b) of **2DySeCN-193**.

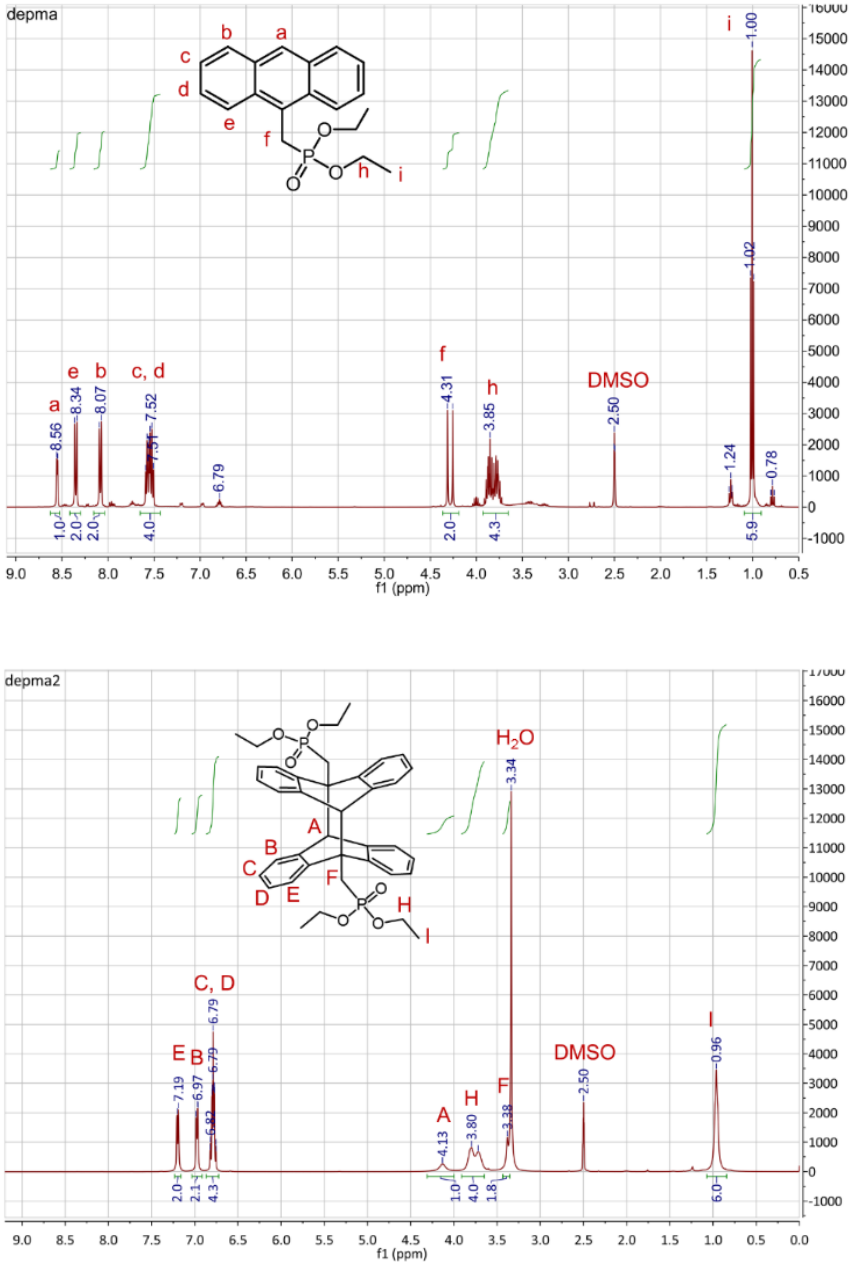

Figure S9. The ^{1}H NMR spectra of pure ligands depma (top) and depma$_2$ (bottom) in DMSO-d6.

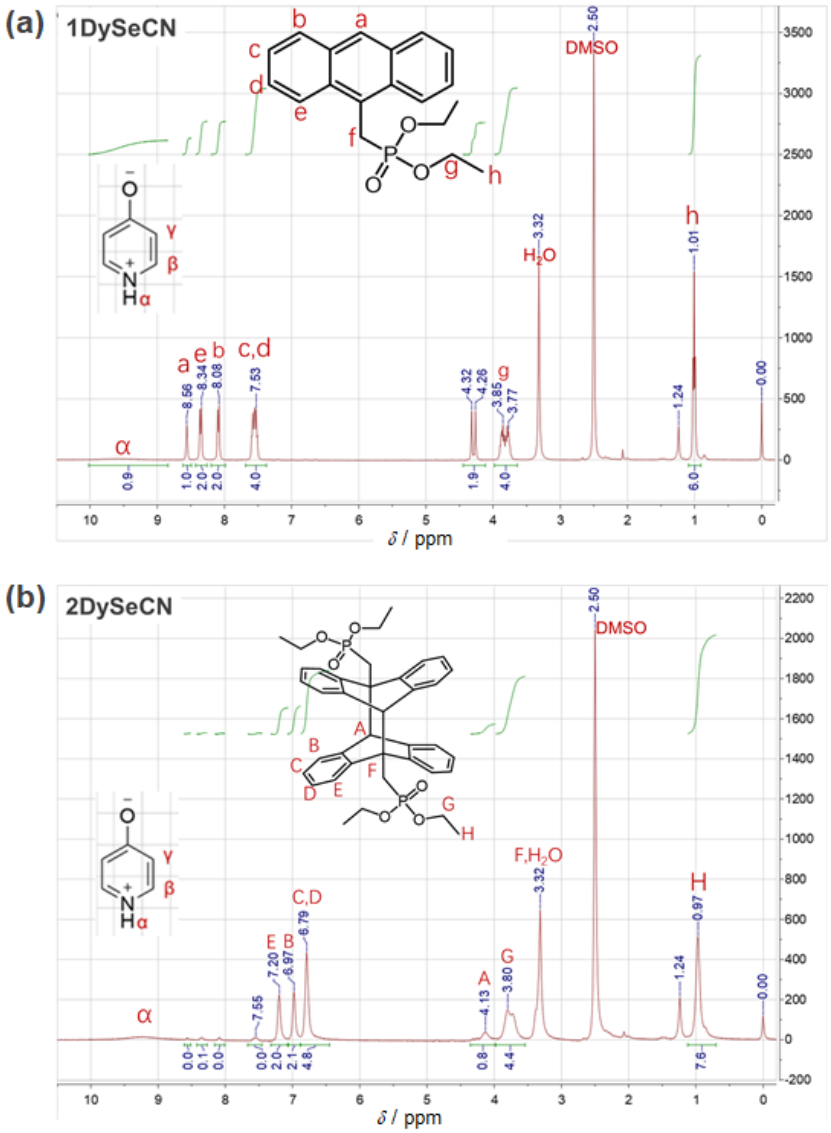

Figure S10. The ^{1}H NMR spectrum of **1DySeCN** (a) and **2DySeCN** (b) in DMSO-d6. The irradiation of **1DySeCN** upon 395 nm UV light for 12 hours gave the sample **2DySeCN**.

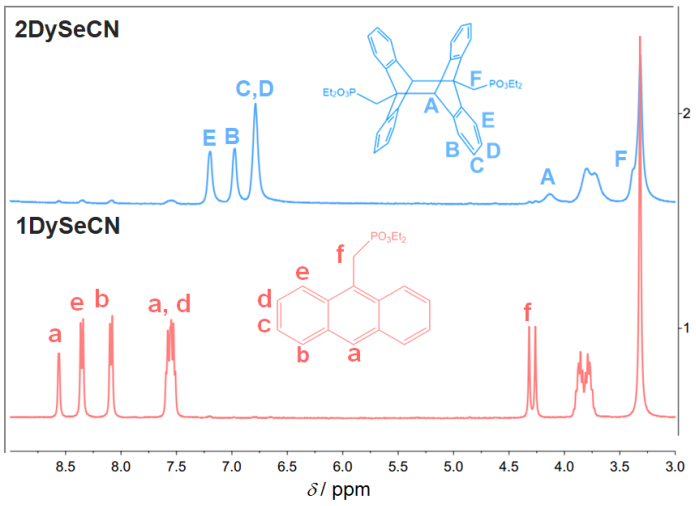

Figure S11. The ^{1}H NMR spectrum in range of 9.0-3.0 ppm of **1DySeCN** and **2DySeCN** in DMSO-d6. The irradiation of **1DySeCN** upon 395 nm UV light for 12 hours gave the sample **2DySeCN**.

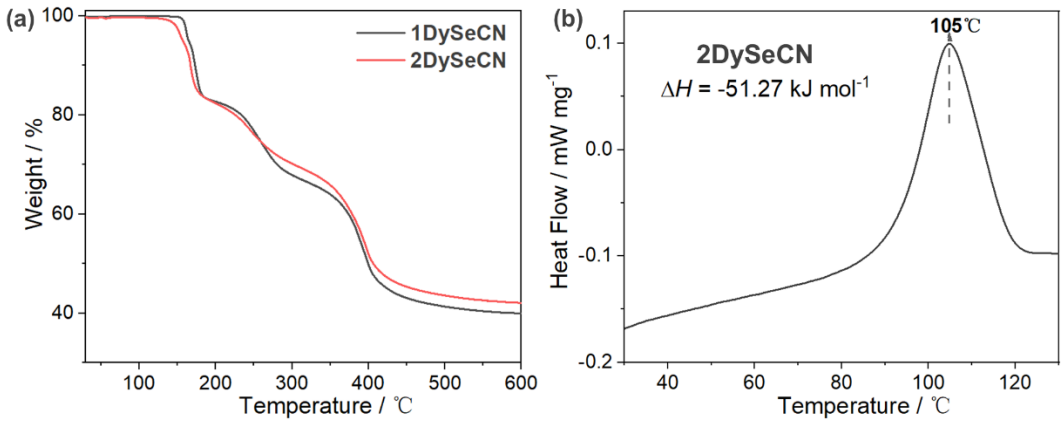

Figure S12. (a) Thermogravimetric (TG) curves for **1DySeCN** and **2DySeCN** measured under nitrogen atmosphere at a heating rate of 5 °C/min; (b) The DSC curve of **2DySeCN** measured under nitrogen atmosphere at a heating rate of 5 °C/min with a strong exothermic peak at 105 °C. The irradiation of **1DySeCN** upon 395 nm UV light for 12 hours gave the sample **2DySeCN**.

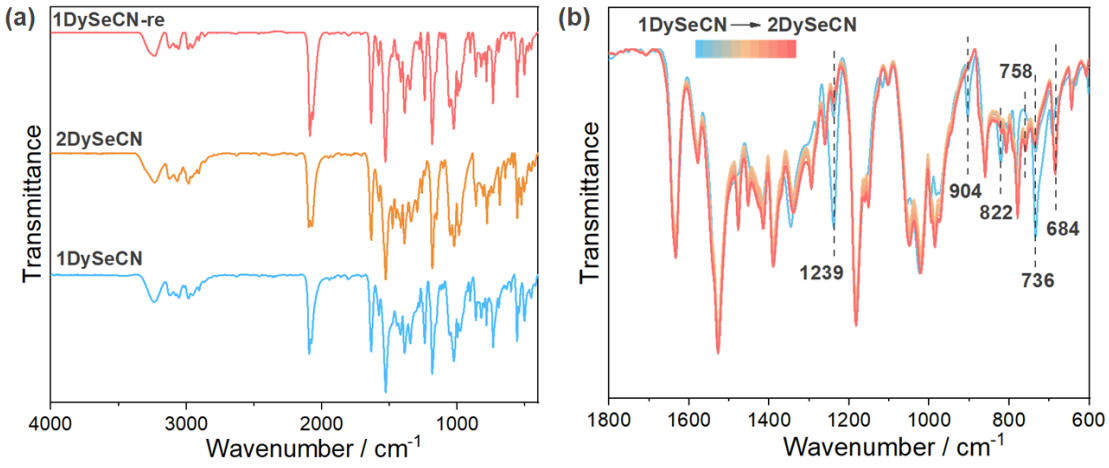

Figure S13. (a)The IR spectra for samples **1DySeCN**, **2DySeCN**, **1DySeCN-re** shown in wavenumber range of 4000-400 cm^{-1}; (b) The time-dependent in-situ IR spectra for **1DySeCN** exposed to 395 nm UV light shown in range of 1800- 600 cm^{-1}. The irradiation of **1DySeCN** upon 395 nm UV light for 12 hours gave the sample **2DySeCN**.

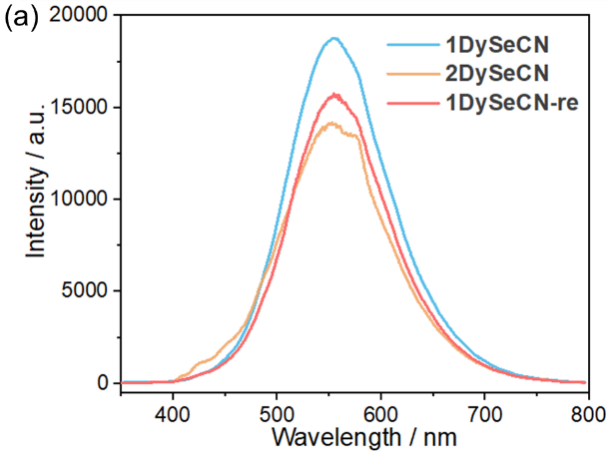

Figure S14. The emission spectra excited at 365 nm for **1DySeCN**, **2DySeCN** and **1DySeCN-re**. The irradiation of **1DySeCN** upon 395 nm UV light for 12 hours gave the sample **2DySeCN**. **1DySeCN-re** formed by heating **2DySeCN** at 105°C for 30 min.

IV. Effect of temperature on the photophysical and photochemical properties of 1DySeCN

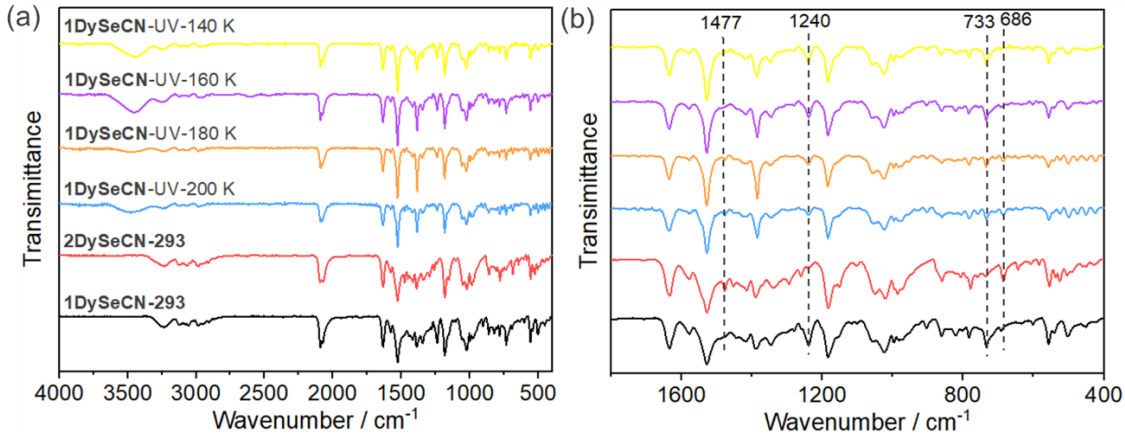

Figure S15. (a)The IR spectra for **1DySeCN** irradiated in situ with 395 nm UV light for 30 min at different temperatures (140-200 K) shown in wavenumber range of 4000-400 cm^{-1}; (b) The IR spectra for **1DySeCN** irradiated in situ with 395 nm UV light for 30 min at different temperatures (140-200 K) shown in range of 1800-400 cm^{-1}.

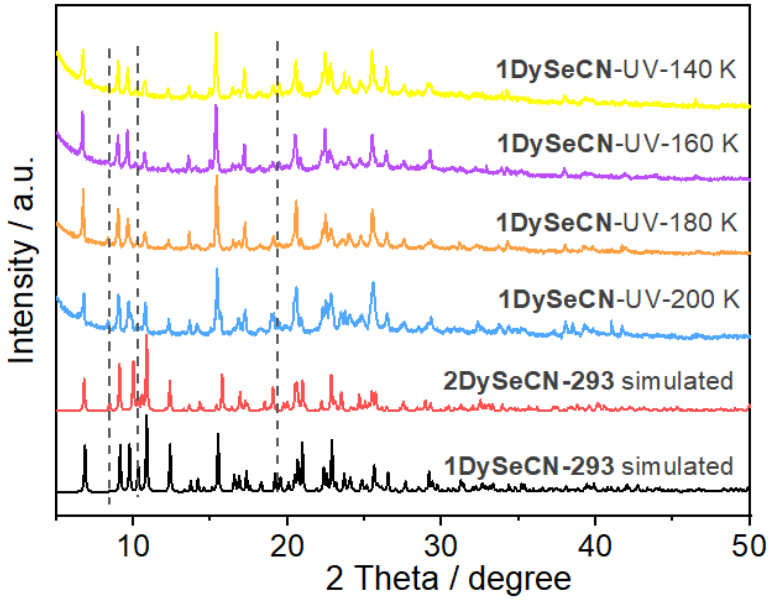

Figure S16. The PXRD patterns for powder samples for **1DySeCN** irradiated in situ with 395 nm UV light for 30 min at different temperatures (140-200 K).

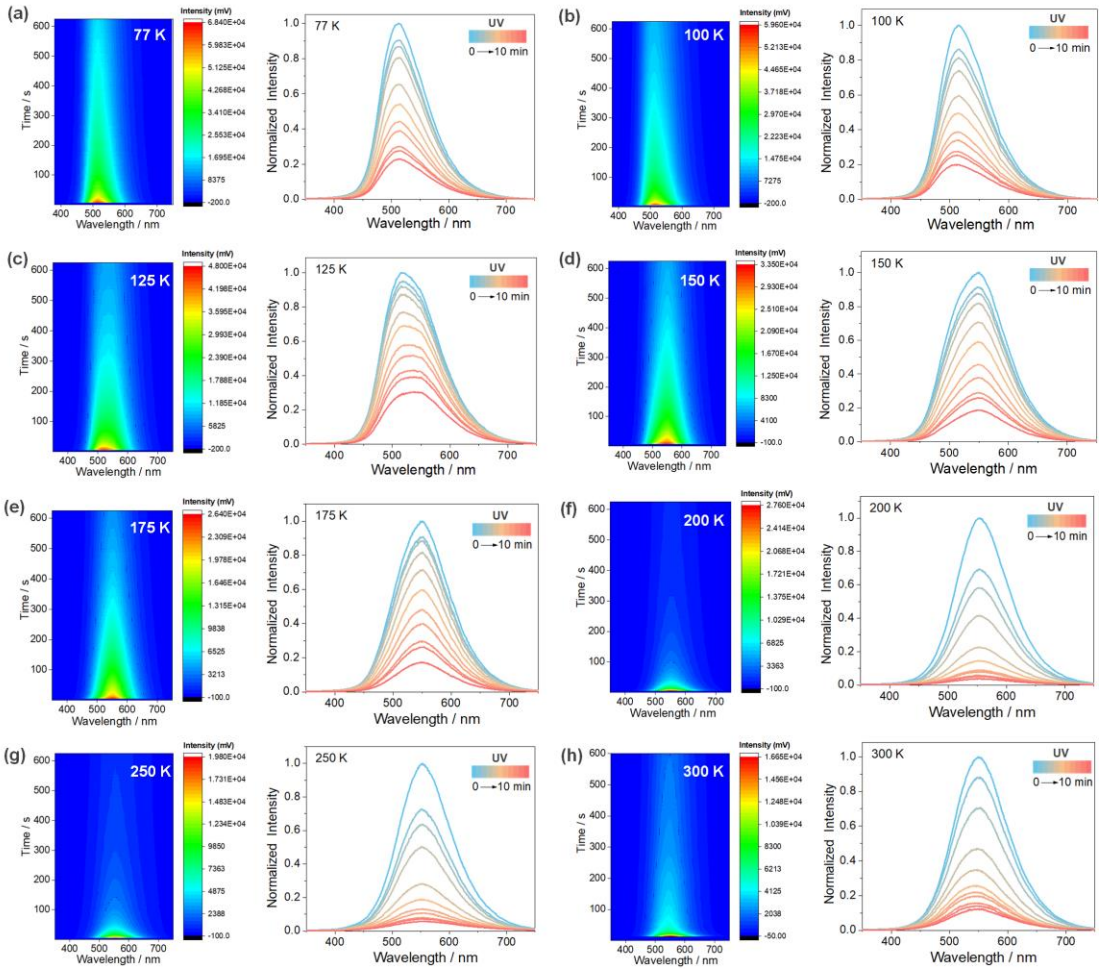

Figure S17. Right: Time-dependent photoluminescence spectra of **1DySeCN@Y** in the range 77-300 K under excitation of 375 nm. Left: photoluminescence spectra at different times (1s, 3s, 5s, 10 s, 30 s, 1 min, 2 min, 3 min, 5 min, 7 min, 10 min) represent the photodimerization process after UV irradiation.

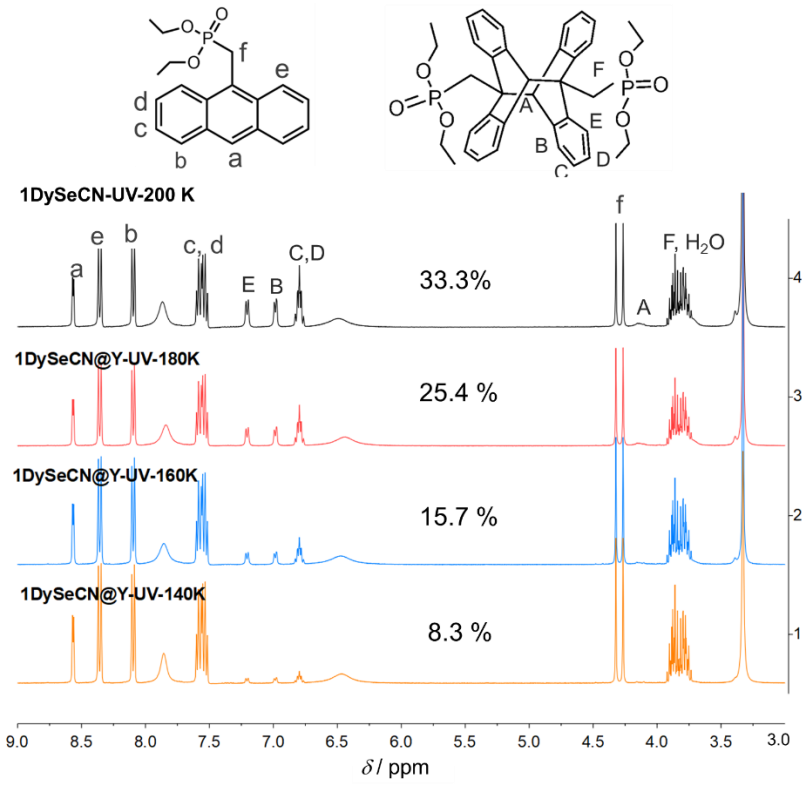

Figure S18. The ^{1}H NMR spectra in range of 9.0-3.0 ppm of **1DySeCN@Y** irradiated in situ with 395 nm UV light for 2 h at different temperatures (140-200 K) in DMSO-d_6.

V. Photo-switchable magnetic properties of 1DySeCN

Table S7. Parameters for magnetic switching in photo-responsive luminescent Ln-SMMs.

Compound	Reversibility	U_{eff} / K	τ_0 / s	T_B / K	ref
Anthracene-based Ln-SMMs					
1	Yes	277	7.2×10^{-11}	4	5
1UV	Yes	139	7.6×10^{-9}	3	
1@Y	Yes	279	6.6×10^{-11}	3.8	
1@Y-UV	Yes	206	8.3×10^{-11}	2.6	
1DySeCN	Yes	**334.1**	1.5×10^{-11}	**4**	This work
2DySeCN	Yes	143.6	6.2×10^{-8}	3	
1DySeCN@Y	Yes	**347.1**	5.9×10^{-12}	**4.2**	
2DySeCN@Y	Yes	207.6	1.4×10^{-9}	3.4	
2	Yes	141	1.1×10^{-9}	\	6
2UV	Yes	101	1.0×10^{-9}	\	
3	Yes	20.4 (500 Oe)	1.5×10^{-8}	\	7
3UV	Yes	43.2 (500 Oe)	5.1×10^{-9}	\	
4	Yes	55.9	1.9×10^{-9}	\	8
4UV	Yes	116	3.7×10^{-11}	\	
5	Yes	117.7	1.4×10^{-8}	\	9
5UV	Yes	172.0	5.1×10^{-11}	\	
6	Yes	48.4 / 110.8	3.0×10^{-8} 1.2×10^{-9}	\	
6UV	Yes	120.5	8.4×10^{-10}	\	
POM-based Ln-SMM					
7	No	19.9	4.2×10^{-7}	\	10
Macrocycle-based Ln-SMM					
8	No	37.8	4.7×10^{-7}	\	11
Viologens-based Ln-SMMs					
9	Yes	off			12
9a	Yes	107.9	1.5×10^{-9}	\	
10	Yes	16.8	8.4×10^{-6}	\	13
10a	Yes	off			
11	Yes	12.1	8.1×10^{-6}	\	
11a	Yes	off			

1 = $[Dy(SCN)_2(NO_3)(depma)_2(4\text{-hpy})_2]$, **1UV** = $[Dy(SCN)_2(NO_3)(depma_2)(4\text{-hpy})_2]_n$ (depma = 9-diethylphosphonomethylanthracene, 4-hpy = 4-hydroxypyridine); **2 =** $[Dy(SCN)_3(depma)_2(4\text{-hpy})_2]$, **2UV =** $[Dy(SCN)_3(depma_2)(4\text{-hpy})_2]_n$; **3 =** $Dy(depma)(NO_3)_3(hmpa)_2$ (hmpa = hexamethylphosphoramide); **4** = $[Dy_2(SCN)_4(L1)_2(dmpma)_4]$ (HL = 4-methyl-2,6-dimethoxyphenol, dmpma= dimethylphosphonomethylanthracene); **5**= $[Dy_2(SCN)_4(L)_2(dmpma)_2(H_2O)_2]$, **5UV** = $[Dy_2(SCN)_4(L)_2(dmpma_2)(H_2O)_2]_n$ (HL = 2,6-dimethoxyphenol); **6** = $[Dy_2(SCN)_4(L2)_2(dmpma)_2(H_2O)_2]$, **6UV** = $[Dy_2(SCN)_4(L)_2(depma_2)(H_2O)_2]_n$; **7** = $N(CH_3)_4]_6K_3H_7[Dy(C_4H_2O_6)(a\text{-}PW_{11}O_{39})]_2{\cdot}27H_2O$; **8** = $[Ln(L^{N6})(NO_3)_2](BPh_4)$ (L^{N6} = (3*E*,5*E*,10*E*,12*E*)-3,6,10,13-tetraaza-1,8(2,6)-dipyridinacyclotetradecaphane-3,5,10,12-tetraene; **9** = $[Dy_3(H\text{-}HEDP)_3(H_2\text{-}HEDP)_3]{\cdot}2H_3\text{-}TPT{\cdot}H_4\text{-}HEDP{\cdot}10H_2O$ (HEDP = hydroxyethylidene diphosphonate; TPT = 2,4,6-tri(4-pyridyl)-1,3,5-triazine); **10** = $[Dy_3(H\text{-}HEDP)_2(H_2\text{-}HEDP)_2(H_3\text{-}HEDP)_2]{\cdot}H_3\text{-}TPP{\cdot}11H_2O$, **11** = $[Tb_3(H\text{-}HEDP)_2(H_2\text{-}HEDP)_2(H_3\text{-}HEDP)_2]{\cdot}H_3\text{-}TPP{\cdot}11H_2O$;

Table S8. The fit parameters obtained from analyses of the ac susceptibilities of **1DySeCN** under zero bias dc field.

T / K	χ_T / cm^3	χ_S / cm^3	ln(τ / s)	α	$R^2 \times 10^{-3}$
2	7.44	0.63	-2.99	0.40	19.4
2.5	5.70	0.53	-3.04	0.39	10.7
3	4.67	0.46	-3.09	0.39	7.14
3.5	3.99	0.42	-3.05	0.37	0.99
4	3.40	0.37	-3.14	0.37	6.77
4.5	3.02	0.34	-3.21	0.36	3.70
5	2.71	0.32	-3.20	0.36	3.93
5.5	2.45	0.30	-3.33	0.35	3.25
6	2.30	0.28	-3.55	0.35	3.92
6.5	2.06	0.26	-3.75	0.35	3.29
7	1.90	0.25	-4.11	0.33	1.06
7.5	1.80	0.24	-4.43	0.33	0.84
8	1.64	0.23	-4.72	0.31	1.24
9	1.43	0.21	-5.04	0.27	0.97
10	1.30	0.20	-5.44	0.24	2.27
11	1.13	0.19	-5.83	0.18	2.23
12	1.00	0.18	-6.33	0.15	1.13
13	0.92	0.17	-6.94	0.13	1.75
14	0.86	0.16	-7.61	0.12	2.17
15	0.79	0.16	-8.33	0.11	2.27
16	0.75	0.16	-9.21	0.12	1.18
17	0.70	0.16	-2.99	0.11	1.81
18	0.66	0.17	-3.04	0.11	2.41
19	0.63	0.17	-3.09	0.13	1.56
20	0.59	0.18	-3.05	0.11	1.20
21	0.57	0.14	-3.14	0.14	0.96
22	0.54	9.05067E-6	-3.21	0.14	0.84

Table S9. The fit parameters obtained from analyses of the ac susceptibilities of **2DySeCN** under zero bias dc field.

T / K	χ_T / cm^3	χ_S / cm^3	ln(τ / s)	α	R^2
2	6.19	0.91	-4.49	0.32	0.18
2.5	4.99	0.76	-4.52	0.32	8.33×10^{-2}
3	4.11	0.66	-4.59	0.31	6.51×10^{-2}
3.5	3.56	0.59	-4.60	0.31	5.07×10^{-2}
4	2.99	0.53	-4.72	0.30	3.55×10^{-2}
4.5	2.74	0.48	-4.70	0.30	2.75×10^{-2}
5	2.44	0.45	-4.77	0.29	1.84×10^{-2}
5.5	2.23	0.41	-4.77	0.30	2.45×10^{-2}
6	2.04	0.39	-4.83	0.28	1.42×10^{-2}
6.5	1.88	0.37	-4.89	0.27	1.46×10^{-2}
7	1.74	0.35	-4.93	0.26	1.41×10^{-2}
7.5	1.61	0.34	-5.02	0.24	1.41×10^{-2}
8	1.49	0.32	-5.13	0.21	1.38×10^{-2}
9	1.32	0.30	-5.29	0.20	6.69×10^{-3}
10	1.20	0.27	-5.46	0.18	6.51×10^{-3}
11	1.08	0.25	-5.71	0.15	4.23×10^{-3}
12	0.98	0.23	-6.01	0.15	2.58×10^{-3}
13	0.90	0.22	-6.39	0.15	2.53×10^{-3}
14	0.85	0.20	-6.90	0.19	2.68×10^{-3}

Table S10. The fit parameters obtained from analyses of the ac susceptibilities of **1DySeCN @Y** under zero bias dc field.

T / K	χ_T / cm^3	χ_S / cm^3	ln(τ / s)	α	$R^2 \times 10^{-3}$
9	1.31	0.05	-1.75	0.15	3.62
9.5	1.13	0.05	-2.22	0.10	4.62
10	1.15	0.05	-2.48	0.11	4.73
105	1.03	0.05	-2.84	0.07	5.39
11	0.99	0.05	-3.09	0.06	6.17
11.5	0.94	0.04	-3.37	0.07	5.59
12	0.90	0.05	-3.62	0.05	8.03
12.5	0.87	0.04	-3.83	0.08	5.16
13	0.81	0.04	-4.16	0.04	6.97
13.5	0.78	0.04	-4.39	0.05	6.80
1	0.74	0.04	-4.61	0.05	3.92
14.5	0.72	0.04	-4.85	0.05	5.50
15	0.71	0.04	-5.09	0.06	3.89
15.5	0.68	0.04	-5.37	0.05	5.88
16	0.66	0.04	-5.65	0.07	4.45
17	0.63	0.04	-6.32	0.08	5.68
18	0.58	0.05	-7.09	0.06	3.75
19	0.55	0.05	-7.90	0.10	8.48
20	0.52	0.07	-8.66	0.08	4.46

Table S11. The fit parameters obtained from analyses of the ac susceptibilities of **2DySeCN@Y** under zero bias dc field.

T / K	χ_T / cm^3	χ_S / cm^3	ln(τ / s)	α	$R^2 \times 10^{-3}$
6	1.09	0.07	-1.13	0.33	2.78
7	0.78	0.06	-2.28	0.26	1.90
8	0.67	0.06	-2.95	0.22	88.6
9	0.58	0.05	-3.58	0.19	1.37
10	0.54	0.05	-4.04	0.20	1.14
10.5	0.53	0.04	-4.21	0.23	2.11
11	0.51	0.04	-4.46	0.21	1.25
11.5	0.48	0.041	-4.71	0.21	1.01
12	0.45	0.04	-5.02	0.21	1.18
12.5	0.43	0.05	-5.28	0.20	1.07
13	0.42	0.04	-5.57	0.23	1.22
13.5	0.42	0.04	-5.82	0.27	1.39
14	0.40	0.03	-6.19	0.30	2.71
14.5	0.38	0.03	-6.62	0.32	1.98
15	0.37	0.04	-6.99	0.34	1.41
15.5	0.36	0.03	-7.39	0.36	2.88
16	0.35	0.04	-7.70	0.40	2.62
16.5	0.33	0.08	-7.88	0.34	4.09
17	0.32	0.11	-7.98	0.33	2.48
17.5	0.31	0.11	-8.28	0.35	2.05
18	0.30	0.15	-8.05	0.25	1.63

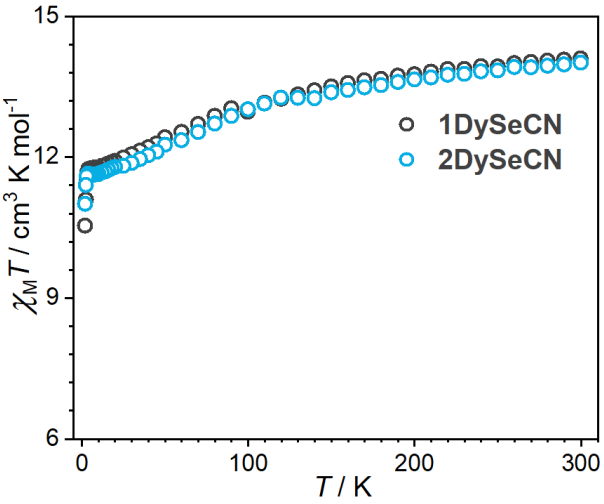

Figure S19. Variable-temperature dc susceptibility data for **1DySeCN** and **2DySeCN** in a 1000 Oe applied dc field.

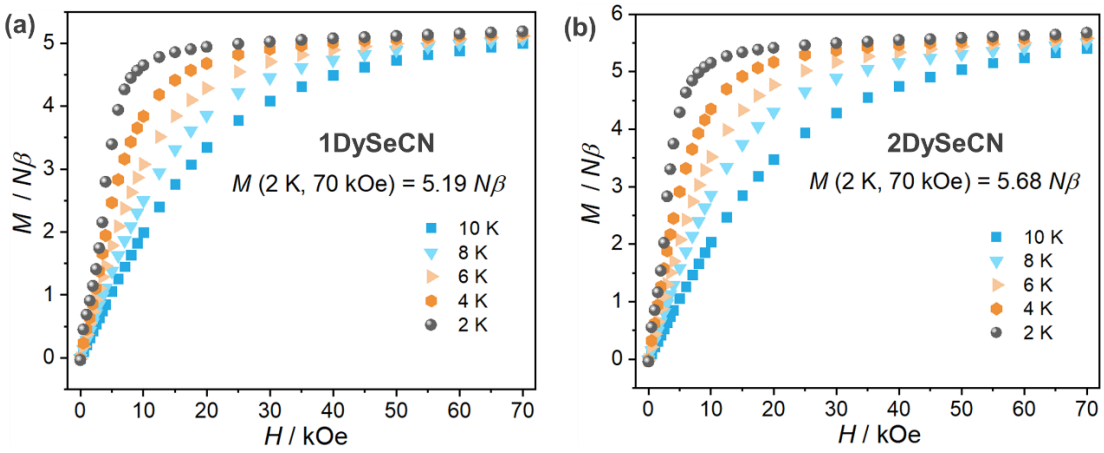

Figure S20. The isothermal magnetization as a function of *H* at depicted temperatures for compounds **1DySeCN**(a) and **2DySeCN** (b).

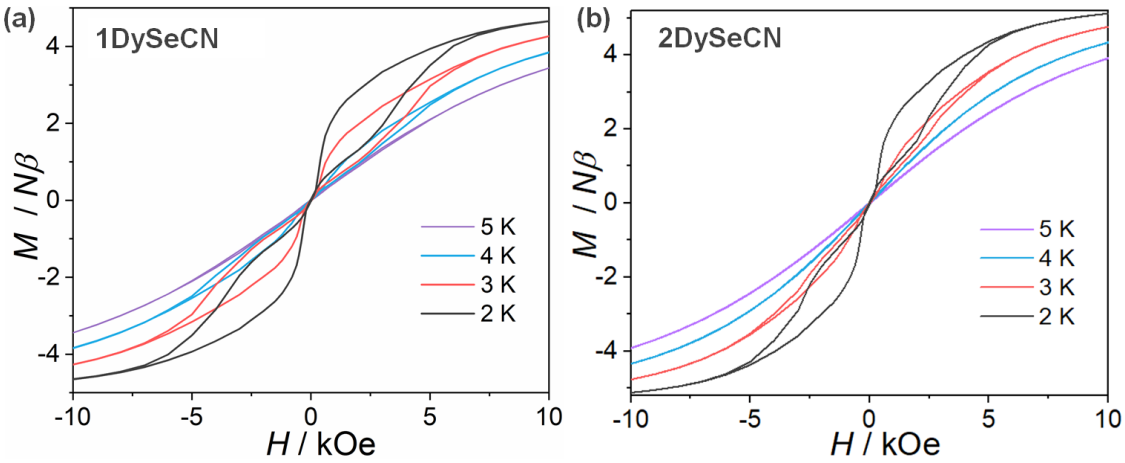

Figure S21. The hysteresis curves for **1DySeCN**(a) and **2DySeCN** (b) below 5 K.

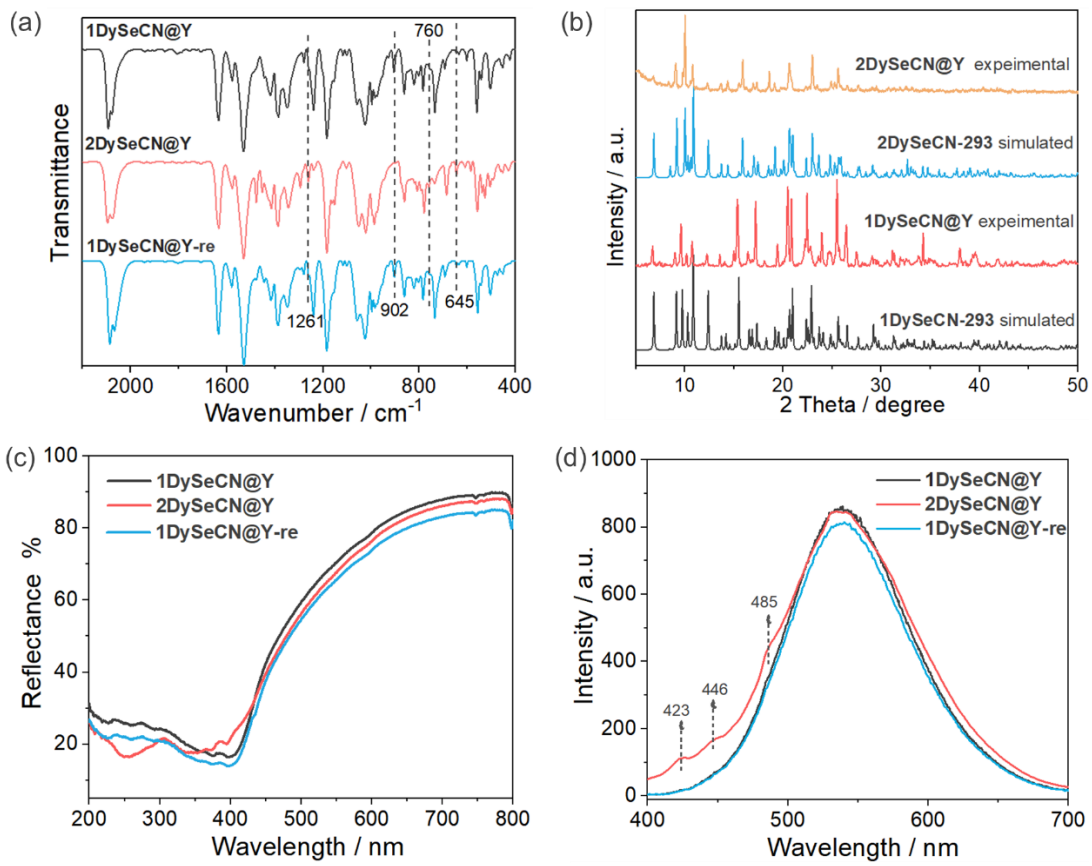

Figure S22. (a)The IR spectra for samples **1DySeCN@Y**, **2DySeCN@Y** and **1DySeCN@Y -re** shown in wavenumber range of 2500-400 cm^{-1}; (b) The PXRD patterns for powder samples of **1DySeCN@Y**, **2DySeCN@Y** compared with their simulated patterns from corresponding crystal structure; (c) The UV-Vis diffused reflectance spectra for compounds **1DySeCN@Y**, **2DySeCN@Y** and **1DySeCN@Y-re** under room temperature; (d) The emission spectra excited at 395 nm for **1DySeCN@Y**, **2DySeCN@Y** and **1DySeCN@Y-re**.

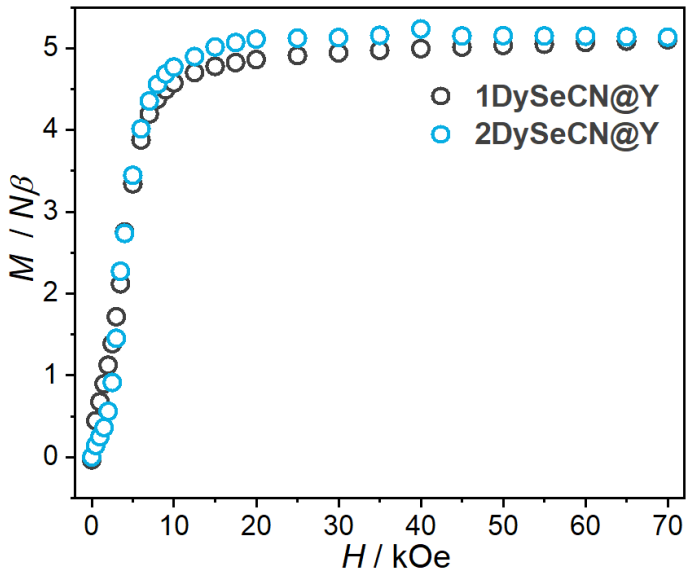

Figure S23. The isothermal magnetization for compounds **1DySeCN@Y** and **2DySeCN@Y**.

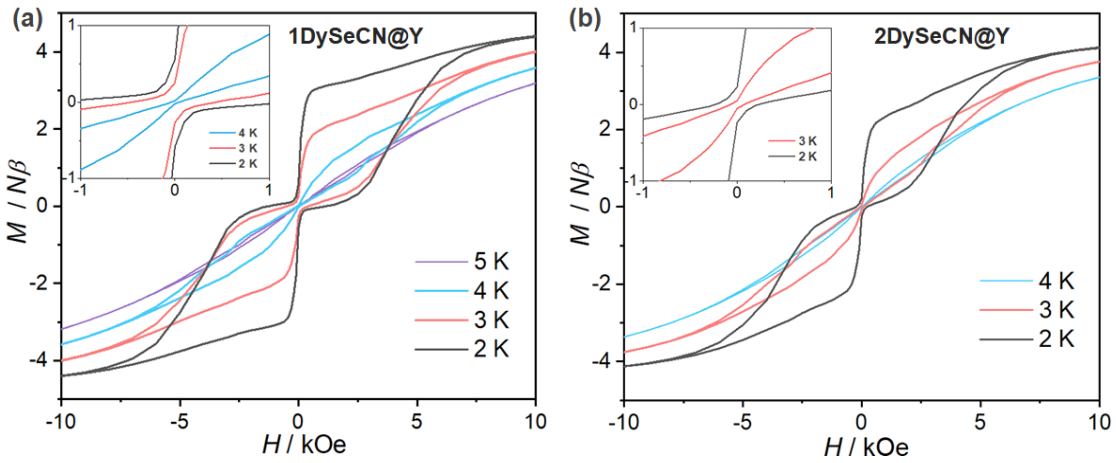

Figure S24. The hysteresis curves for **1DySeCN@Y**(a) and **2DySeCN@Y** (b) below 5 K.

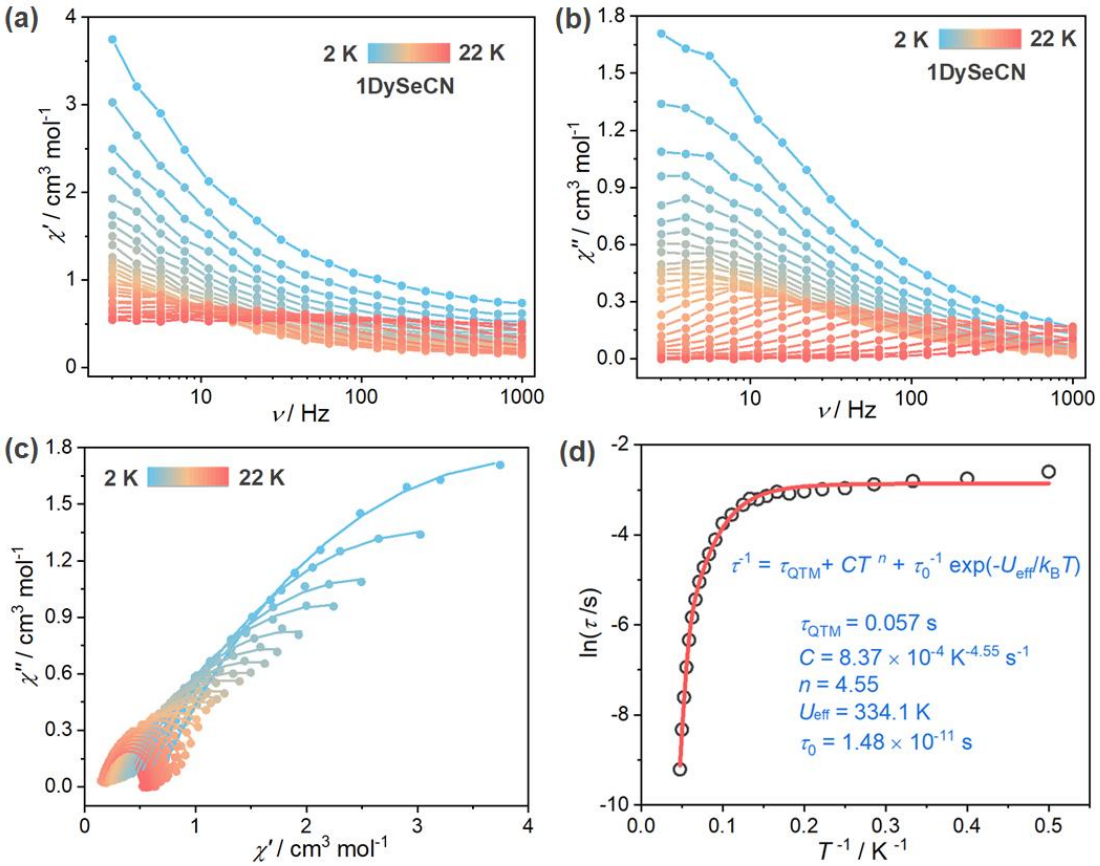

Figure S25. (a,b) Frequency dependent in-phase (χ') and out-of-phase (χ'') ac susceptibilities of **1DySeCN** under zero dc fields. c) The corresponding Cole-Cole plots of **1DySeCN**. The solid lines are the best fits with generalized Debye model. d) The plot of $\ln\tau$ vs. T^{-1} for **1DySeCN** measured at zero dc fields.

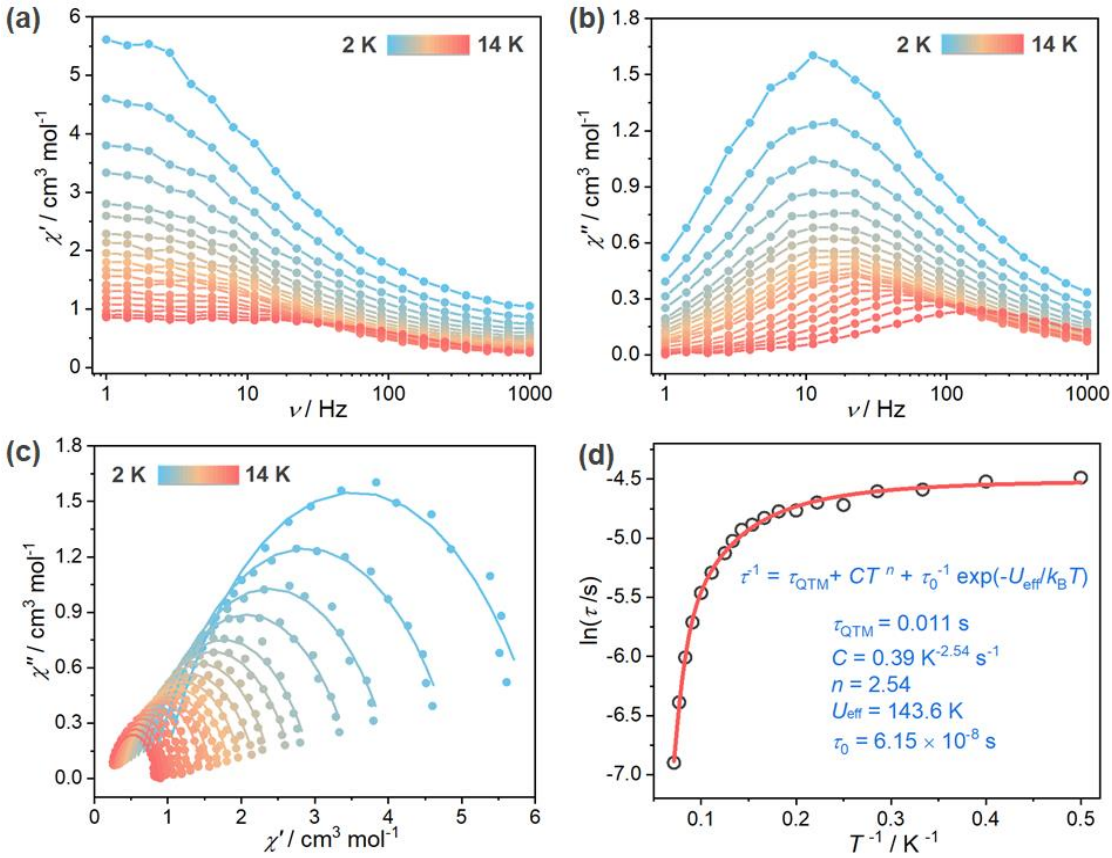

Figure S26. (a,b) Frequency dependent in-phase (χ') and out-of-phase (χ'') ac susceptibilities of **2DySeCN** under zero dc fields. c) The corresponding Cole-Cole plots of **2DySeCN**. The solid lines are the best fits with generalized Debye model. d) The plot of $\ln\tau$ vs. T^{-1} for **2DySeCN** measured at zero dc fields.

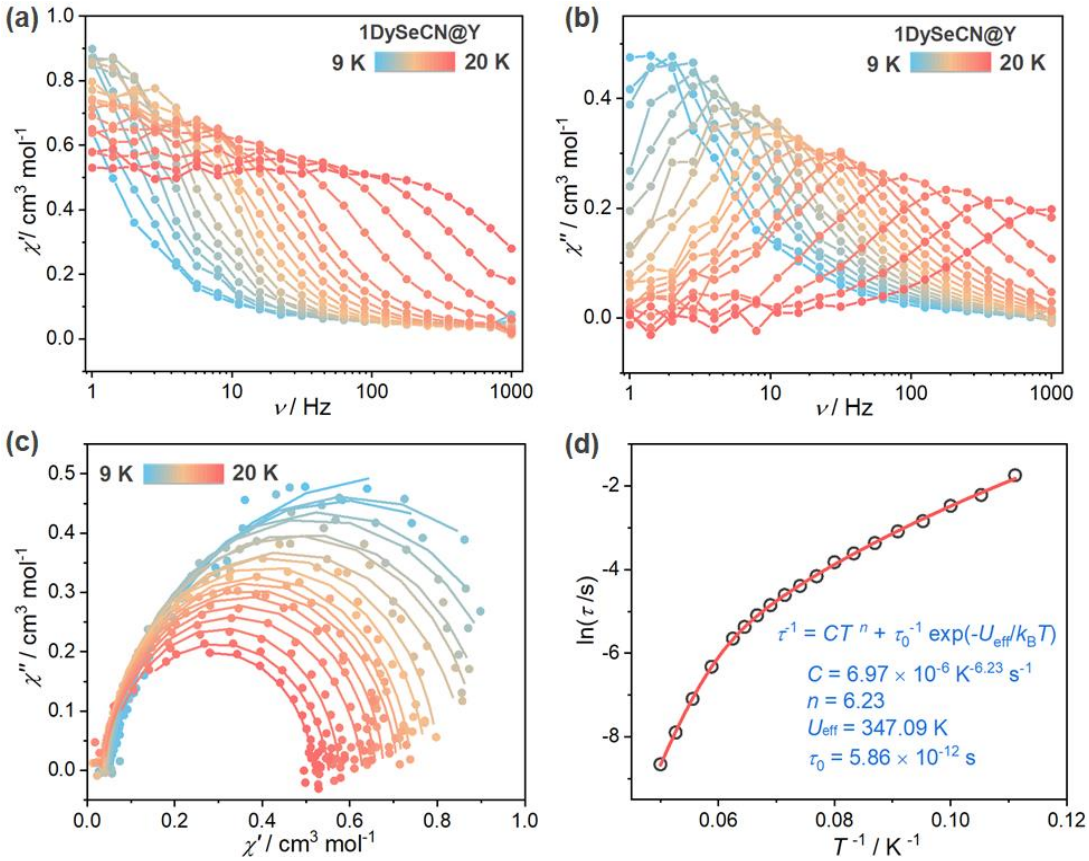

Figure S27. (a,b) Frequency dependent in-phase (χ') and out-of-phase (χ'') ac susceptibilities of **1DySeCN@Y** under zero dc fields. c) The corresponding Cole-Cole plots of **1DySeCN@Y**. The solid lines are the best fits with generalized Debye model. d) The plot of $\ln\tau$ vs. T^{-1} for **1DySeCN@Y** measured at zero dc fields.

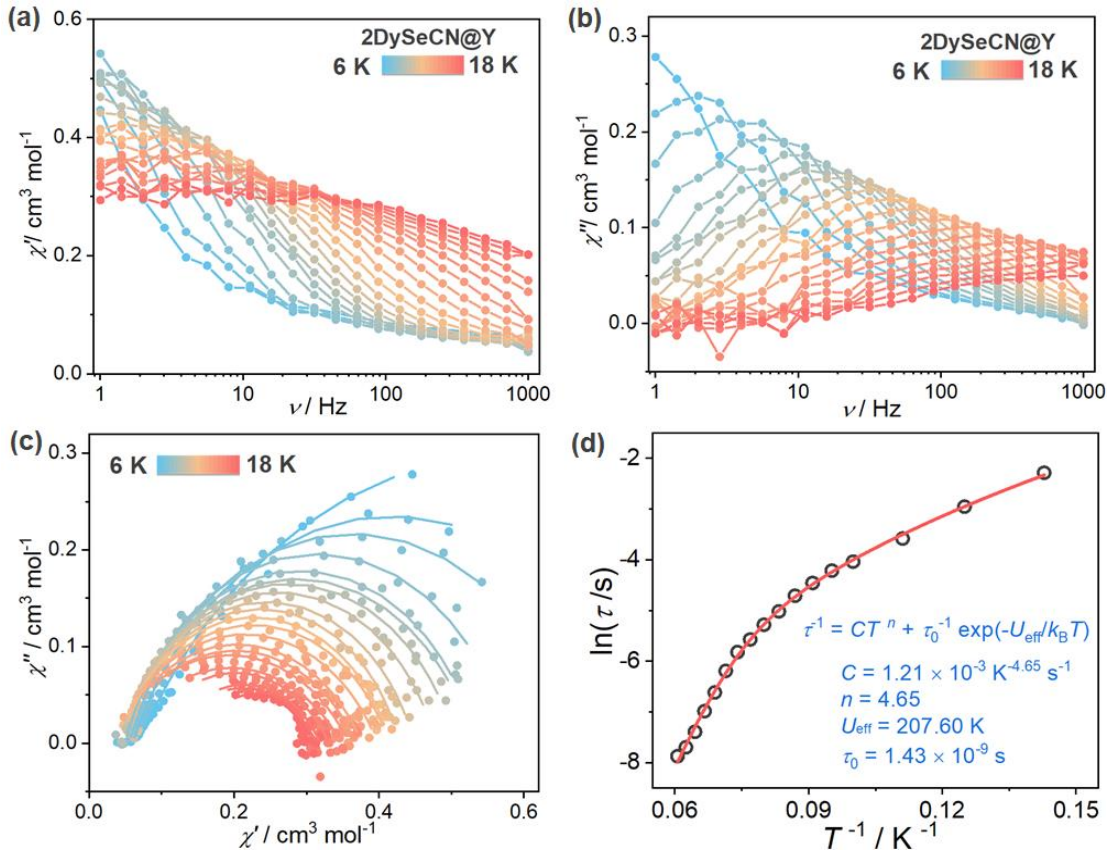

Figure S28. (a,b) Frequency dependent in-phase (χ') and out-of-phase (χ'') ac susceptibilities of **2DySeCN@Y** under zero dc fields. c) The corresponding Cole-Cole plots of **2DySeCN@Y**. The solid lines are the best fits with generalized Debye model. d) The plot of lnτ vs. T^{-1} for **2DySeCN@Y** measured at zero dc fields.

VI. References

1 D.-K. Cao, Y.-W. Gu, J.-Q. Feng, Z.-S. Cai and M. D. Ward, *Dalton Trans.*, 2013, **42**, 11436–11444.

2 O. Kahn, Molecular Magnetism, Wiley-VCH: New York., 1993.

3 SAINT, Program for Data Extraction and Reduction, Siemens Analytical X-ray Instruments, Madison, WI, 1994–1996.

4 (a) O. V. Dolomanov, L. J. Bourhis, R. J. Gildea, J. A. K. Howard and H. Puschmann, *J. Appl. Cryst.*, 2009, **42**, 339–341; (b) L. Krause, R. Herbst-Irmer, G.M. Sheldrick and D. Stalke, *J. Appl. Cryst.*, 2015, **48**, 3–10.

5 X.-D. Huang, X.-F. Ma and L.-M. Zheng. *Angew. Chem. Int. Ed*. 2023, **62**, e202300088.

6 X.-D. Huang, G.-H. Wen, S.-S. Bao, J.-G. Jia and L.-M. Zheng, *Chem. Sci.* 2021, **12**, 929−937.

7 X.-D. Huang, Y. Xu, K. Fan, S.-S. Bao, M. Kurmoo and L.-M. Zheng, *Angew. Chem. Int. Ed.* 2018, ***57,*** 8577–8581.

8 X.-D. Huang, X.-F. Ma, T. Shang, Y.-Q. Zhang and L.-M. Zheng, *Inorg. Chem.,* 2023, 62, 1864–1874.

9 X.-F. Ma, X.-D. Huang and L.-M. Zheng. *Cryst. Growth Des*. 2023, **23**, 1095−1103.

10 P.-T. Ma, F. Hu, R. Wan, Y. Huo, D.-D. Zhang, J.-Y. Niu and J.-P. Wang, *J. Mater. Chem. C,* 2016, **4**, 5424--5433

11 P.-Y. Liao, Y. Liu, Z.-Y. Ruan, H.-L. Wang, C.-G. Shi, W. Deng, S.-G. Wu, J.-H. Jia and M.-L. Tong, *Inorg. Chem*. 2023, **62**, 1075−1085.

12 Y.-J. Ma, J.-X. Hu, S.-D. Han, J. Pan, J.-H. Li and G.-M. Wang, *J. Am. Chem. Soc*. 2020, **142**, 2682−2689.

13 Q. Zhang, S.-D. Han, Q. Li, J.-X. Hu and G.-M. Wang, *Sci China Mater*, 2022, **65**, 788–794.